Evaluation of the air-sea bulk formula and sea-surface temperature variability from observations

Dean Vickers[1] and L. Mahrt[1]

Received 27 September 2005; revised 2 January 2006; accepted 24 January 2006; published 2 May 2006.

[1] Eddy-correlation fluxes are compared to air-sea fluxes predicted by a widely used bulk flux formulation without wave-state effects. Systematic discrepancies are found. For example, the model approximately equates the roughness lengths for heat and moisture; however, the observed roughness length for heat (z_{oh}) exceeds that for moisture (z_{oq}) by an order of magnitude or more, except in the strongest wind-speed conditions. This is apparently due to the dynamic nature of temperature, which dominates buoyancy generation of turbulence in these data sets. The observed correlation between temperature and vertical velocity fluctuations generally exceeds that for moisture. For 10-m wind speeds above a threshold value of 12 m s^{-1}, z_{oq} exceeds z_{oh} apparently owing to enhanced moisture flux associated with the onset of wave breaking coupled with advection of cold dry air from land. In near-collapsed turbulence, the observed momentum flux is smaller than predicted, and there is no clear indication of a smooth flow viscous regime. The scatter between observed and bulk fluxes generally decreases with averaging the observed fluxes over greater length scales even with variations in sea-surface temperature (SST). The reduction in random flux sampling errors more than compensates for capturing increased surface heterogeneity with increasing averaging scale. Since similarity theory does not apply to heterogeneous surfaces, the bulk model does break down in the extreme case where the averaging window includes a sharp SST front. The response of the flow to changes in SST is presented for different amplitudes of SST variability. The change in vertical structure and acceleration of the low-level wind over warm pools is discussed.

Citation: Vickers, D., and L. Mahrt (2006), Evaluation of the air-sea bulk formula and sea-surface temperature variability from observations, *J. Geophys. Res.*, *111*, C05002, doi:10.1029/2005JC003323.

1. Introduction

[2] Reliable formulation of air-sea fluxes of momentum, sensible heat and latent heat is critical for accurate forecasts of the marine boundary layer. The surface flux is commonly parameterized in large-scale models using a bulk flux formulation in terms of exchange coefficients that depend on stability and roughness lengths [e.g., *Fairall et al.*, 1996; *Mahrt et al.*, 2003]. The stability functions, which include empirical coefficients based on decades of field studies conducted over land, are thought to also apply over the water [*Edson and Fairall*, 1998; *Vickers and Mahrt*, 1999; *Edson et al.*, 2004]. Unlike over land, the roughness lengths depend on time-dependent characteristics of the surface waves. For example, the roughness length for momentum depends on wave age [*Donelan*, 1990; *Maat et al.*, 1991; *Smith et al.*, 1992; *Grachev and Fairall*, 2001; *Drennan et al.*, 2003], although most large-scale atmospheric models do not include information on wave state.

[3] The bulk flux model assumes stationarity and homogeneity such that: (1) the drag coefficient only depends on z/L and z/z_{om} as described by Monin-Obukhov similarity theory where z is height above the surface, L is the Obukhov length scale and z_{om} is the roughness length, (2) the sea-surface roughness is proportional to the momentum transport from the atmosphere to the ocean (e.g., Charnock formulation of z_{om}), and (3) the observations are taken in the surface layer. The latter criteria requires the observations to be above the wave boundary layer [e.g., *Hare et al.*, 1997] yet low enough in the atmospheric boundary layer that the change in the flux with height below the measurement level can be ignored. Despite these requirements, large-scale models must apply the bulk flux formulation in all conditions, as there is no viable alternative. This contributes to discrepancies between modeled and observed fluxes.

[4] In this study, eddy-correlation fluxes from aircraft and tower measurements over the ocean are compared to flux estimates from a widely used bulk flux model without wave-state information. Similar bulk models without wave-state effects are used to parameterize the air-sea fluxes in most large-scale atmospheric models.

[5] The structure of the marine boundary layer is strongly influenced by well-defined large amplitude sea-surface temperature (SST) fronts, such as the edge of the Gulf

[1]College of Oceanic and Atmospheric Sciences, Oregon State University, Corvallis, Oregon, USA.

0148-0227/06/2005JC003323$09.00

stream current in the north Atlantic [*Mahrt et al.*, 2004] and the cold tongue-ITCZ region in the eastern tropical Pacific [*Thum et al.*, 2002; *Pyatt et al.*, 2005]. In the second part of this study, we use aircraft observations to explore the sensitivity of the surface fluxes and low-level mean meteorology to smaller amplitude, more common SST variability.

[6] The measurements and methods used to estimate air-sea fluxes are described in section 2, while the details of the bulk flux model are presented in section 3. Section 4 contrasts bulk and observed fluxes. The response of the marine boundary layer to modest amplitude spatial variability in SST is discussed in section 5, and conclusions follow in section 6.

2. Data

2.1. LongEZ Aircraft

[7] Data collected by the NOAA LongEZ (N3R) aircraft during two field experiments, (1) the pilot program of the Coupled Boundary Layers Air Sea Transfer experiment (CBLAST Weak Wind) conducted over the Atlantic Ocean south of Martha's Vineyard Island, Massachusetts, during July–August 2001, and (2) the Shoaling Waves experiment (SHOWEX) in November and December 1999 over the Atlantic off the Outer Banks near Duck, North Carolina, are used in the analysis. The data were collected at a temporal sampling rate of 50 Hz, corresponding to a spatial sampling interval of 1 m for an aircraft speed of 50 m s^{-1}. Eddy-correlation fluxes were calculated from data collected during low altitude (10 to 20 m) flight segments where aircraft altitude, roll, pitch and heading fluctuations remained within prescribed limits and where the flight track was either primarily into or following the mean wind. The latter criteria enables a better estimate of the SST in the flux footprint, but significantly reduces the size of the data sets. An accurate SST estimate is critical for evaluating fluxes with the bulk model.

[8] SHOWEX data collected very near shore in offshore flow conditions, which were emphasized in previous studies by *Mahrt et al.* [2001] and *Sun et al.* [2001], are excluded from this study; however, this does not imply that land influences are totally removed. Advection can extend the influence of land tens of kilometers or more off the coast [*Smedman et al.*, 1997; *Mahrt et al.*, 2001]. With these restrictions, the SHOWEX data set includes 190 flight segments on 21 different days, while the CBLAST pilot data set includes 74 flight segments on nine different flight days. Individual flight segments refer to continuous segments of the flight that satisfy all the criteria above and are 10 km in length or more. The longest flight segment is 70 km.

[9] LongEZ instrumentation was described in detail by *Crescenti et al.* [1999] and *Sun et al.* [2001]. The LongEZ is a light pusher aircraft with the engine mounted on the rear of the airplane with the large main wing set back farther than that of conventional aircraft. The small, low-drag airframe and rear-mounted pusher engine reduce the influence of flow distortion, engine vibration and engine exhaust for instruments mounted on the nose. Winds are measured using the BAT probe, positioned 2 m in front of the nose and 5 wing-widths ahead of the canard. Fast-response temperature is measured using a 0.13 mm micro-bead thermistor mounted inside the design stagnation point port on the BAT hemisphere. Fast-response humidity is measured using an open-path infrared gas analyzer (IRGA) designed and built by Air Resources Laboratory, NOAA. An EG&G (200) chilled mirror measured slow response dew point temperature.

[10] The aircraft fluxes compare favorably with fluxes measured with eddy-correlation instrumentation on two different buoys and from sonic anemometers deployed on the Duck pier for limited intercomparisons [*Mahrt et al.*, 2001]. The aircraft could underestimate the flux in shallow boundary layers due to significant change in the flux between the surface and the aircraft level. We attempt to correct for this effect in stable conditions (section 2.5).

[11] Another concern is the loss of flux at high frequencies. Owing to the sampling interval of 1 m, all fluxes on horizontal scales less than about 2 m are lost. The flux is lost because the data were filtered to remove noise at small scales, and therefore there is no folding back (aliasing) of flux at small scales to larger scales. Fluctuations of aircraft altitude are a concern as they can lead to artificial fluctuations in the presence of strong mean vertical gradients. Using the LongEZ SHOWEX data, *Mahrt et al.* [2005] found that fluxes of heat and momentum were slightly overestimated owing to this effect in strongly stable flows. This error is expected to offset to some degree underestimation of the flux owing to loss of small-scale fluctuations in stable conditions.

[12] Of concern is the apparent ambient temperature dependence in the Everest Interscience (4000.4GXL) infrared radiometer which measures sea-surface radiative temperature. We adjusted the surface skin temperature measurements from the radiometer for both the SHOWEX and CBLAST pilot experiments. The adjustment consists of applying one constant offset temperature for each flight day derived from comparisons with SST measurements from buoys, and by assuming that the heat flux should be directed down the mean temperature gradient. Plots of the heat flux as a function of the air-sea temperature difference sometimes reveal an offset relative to the zero crossing. We assume that this offset, when present, is due to drift in the calibration of the radiometer, and adjust the SST accordingly.

2.2. Pelican Aircraft

[13] Additional data were collected by the Naval Postgraduate School's CIRPAS (Center of Inter-Disciplinary Remotely Piloted Aircraft Studies) Pelican aircraft in the CBLAST experiment during August 2003. The turbulence group at the University of California at Irving (UCI) (Djamal Khelif and Carl Friehe) installed the instrumentation and data logging systems on the aircraft. CBLAST was the first research project for this combination of aircraft and instrumentation [*Khelif et al.*, 2004].

[14] The nominal low-level altitude for flux measurements was 30 m above the surface. Data were collected at a sampling rate of 40 Hz, corresponding to a sampling interval of about 1.5 m. We applied no corrections to UCI's Version 3.0 data set. After applying criteria based on the allowed variations in aircraft altitude and heading (aircraft roll and pitch data were not available), and requiring the flight track be either into or following the mean wind, the Pelican CBLAST data includes 94 flight segments on 10 different days.

[15] It appears that the Pelican flight altitude (30 m) was too high above the sea surface to capture the fluxes in the weak wind stable conditions in the CBLAST study region during August 2003. The Pelican fluxes are shown in section 4, but are not discussed further.

2.3. Air-Sea Interaction Tower

[16] Data from the Air-Sea Interaction Tower (ASIT) collected during the CBLAST experiment in late summer of 2003 are analyzed [*Edson et al.*, 2004]. The fast-response wind, temperature and humidity data were obtained from Jim Edson of the University of Connecticut (formerly of Woods Hole Oceanographic Institute). The offshore tower is located 3 km south of Martha's Vineyard in 15 m of water. The 20-Hz turbulence measurements collected by a CSAT3 sonic anemometer (Campbell Scientific, Inc.) and a colocated LI-7500 open path gas analyzer (LI-COR, Inc.) at approximately 5 m above the sea surface are used to calculate eddy-correlation fluxes of momentum, sensible heat and latent heat. Slow response measurements include mean air temperature and humidity at multiple levels and sea-surface radiative temperature.

[17] We retain data for analysis only for periods with the wind direction inside the sector from 160 to 250 degrees (flow from the SSW) to avoid influences from nearby land to the north and shallow water to the east and west. This criteria also eliminates periods with flow through the tower prior to reaching the turbulence instruments. Some moisture flux data were discarded due to unphysical behavior of the fast-response humidity from the LI-7500, apparently due to condensation on the lens in high humidity and fog conditions. With these restrictions, the data set includes 383 1-hour averages between 16 July and 2 October 2003. The majority of the retained data are characterized by weak winds and warm air over cooler water.

2.4. Flux Calculations

[18] Two timescales are used to calculate the turbulence flux: (1) τ defines the perturbation quantities and determines what scales of motion contribute to the calculated flux, and (2) λ is the scale over which products of perturbations are averaged. Using too small a window size τ leads to systematic flux loss and underestimation of the flux, while using too large a window inadvertently includes poorly sampled mesoscale motions which can degrade flux-gradient relationships and the performance of the bulk model [*Smedman*, 1988; *Howell and Sun*, 1999; *Vickers and Mahrt*, 2006]. Choice of λ that is too small increases the random flux sampling error, while choice of λ that is too large captures additional heterogeneity (nonstationarity at the tower).

[19] An algorithm is used to identify the averaging timescale τ for each individual flight segment (and each 1-hour record from the tower) that captures the turbulence while excluding most of the mesoscale motions [*Vickers and Mahrt*, 2006]. The method is based on identifying the gap region in the multiresolution heat flux cospectra. The gap scale τ is typically a factor of 5 larger in unstable conditions compared to stable conditions owing to suppression of the larger eddies by the stratification and shallow boundary-layer depth in stable flows.

[20] Once the perturbation quantities are computed on the basis of the averaging scale τ, the fluxes are averaged over a larger window λ. For the aircraft, we compute fluxes for λ windows ranging from 2 to 32 km in length to examine the influences of random flux error and surface heterogeneity. The length scale λ defines the averaging window for the basic mean state quantities U, θ, q and θ_s required for the bulk flux model (section 3). For the ASIT data, we use the variable τ and a constant λ = 1 hour.

2.5. Extrapolation to the Surface

[21] In shallow stable boundary layers, the magnitude of the flux measured at the aircraft level can be significantly less than the surface flux. We account for the change in the flux with height below the aircraft by using a simple parameterization of stable boundary layer depth h [*Donelan*, 1990],

$$h = C\frac{u*}{f}, \tag{1}$$

where u_* is the friction velocity and f is the Coriolis parameter. Variations in the Coriolis parameter have no influence for these data. The nondimensional coefficient C = 0.04 is based on observed stable boundary layer depths inferred from aircraft soundings and air-sea momentum fluxes from low-level flight segments by the LongEZ in the CBLAST pilot experiment [*Vickers and Mahrt*, 2004]. Boundary-layer depth was determined by examining the vertical profile of turbulence energy, potential temperature and wind. The above formulation for h was not the best form evaluated in terms of correlation with the observed h (14 different forms for h were evaluated), but serves our purpose here in that only an estimate of u_* is required.

[22] The flux at aircraft level is extrapolated to the surface by assuming a linear flux profile between the surface and the top of the boundary layer, where the flux is zero. The surface flux F_{sfc} is then calculated from the flux at aircraft level F as

$$F_{sfc} = \frac{h}{(h-z)}F, \tag{2}$$

where F refers to the fluxes of momentum, sensible heat and latent heat and z is aircraft altitude. The modeled h is restricted to be no smaller than the smallest observed stable boundary layer depth of about 50 m. While this adjustment to the flux (equations (1)–(2)) is admittedly crude, it should account for first-order systematic effects due to shallow stable-boundary layers.

[23] No correction is applied when $z/L < 0.1$ where the boundary-layer depth typically exceeds a few hundred meters and the change in the flux between the aircraft level and the surface is presumably small. With this criteria, 30% of the CBLAST pilot experiment 4-km average fluxes are corrected by an average of 18%. The corresponding numbers for the SHOWEX data are 14% of the fluxes with an average correction factor of 32%. For the tower data, we assume negligible flux divergence below the flux measurement level of approximately 5 m and do not apply equations (1)–(2). The flux instruments on the tower were lowered from 6 to 4 m above the surface on 19 August.

3. Bulk Flux Model

[24] Fluxes of momentum (M), sensible heat (H) and latent heat (LE) between the sea surface and the atmosphere

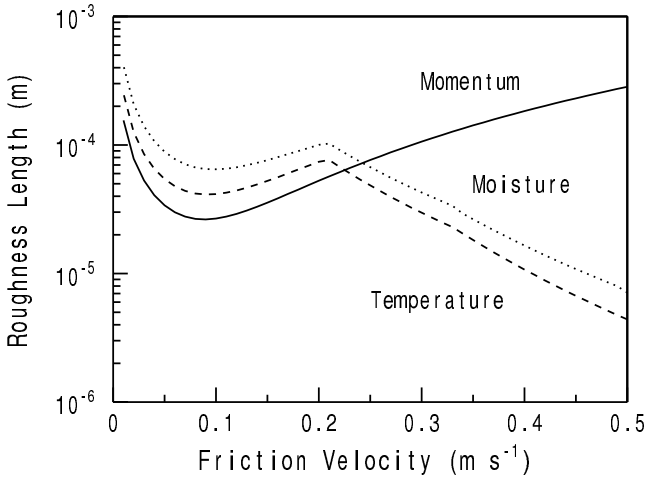

Figure 1. Roughness lengths (meters) specified in the COARE v2.5 bulk model as a function of friction velocity (m s^{-1}).

are formulated in most atmospheric models using standard flux-gradient relationships with stability-dependent exchange coefficients written as

$$M \equiv \rho u_*^2 = \rho C_d U^2 \tag{3}$$

$$H \equiv \rho c_p \overline{w'\theta'} = \rho c_p C_h U(\theta_s - \theta) \tag{4}$$

$$LE \equiv \rho L_v \overline{w'q'} = \rho L_v C_q U(q_s - q). \tag{5}$$

Subscript s denotes the value at the sea surface, while wind speed U, potential temperature θ and specific humidity q are evaluated at height z above the surface. We use a local potential temperature defined as the temperature plus 0.01 z, where z has units of m. Here θ_s is the surface radiative temperature (sea-surface skin temperature) and q_s is the saturated specific humidity at the sea-surface skin temperature. We reduce q_s by 2% to account for the salinity effect [*Sverdrup et al.*, 1942].

[25] The height, stability and roughness length dependent exchange coefficients are given by Monin-Obukhov similarity theory as

$$C_d = \left[\frac{\kappa}{\ln(z/z_{om}) - \psi_m}\right]^2, \tag{6}$$

$$C_h = \left[\frac{\kappa}{\ln(z/z_{om}) - \psi_m}\right]\left[\frac{\kappa}{\ln(z/z_{oh}) - \psi_h}\right], \tag{7}$$

$$C_q = \left[\frac{\kappa}{\ln(z/z_{om}) - \psi_m}\right]\left[\frac{\kappa}{\ln(z/z_{oq}) - \psi_q}\right], \tag{8}$$

where $\kappa = 0.4$ is the von Karmen constant, ψ_m, ψ_h and ψ_q are the stability functions, and z_{om}, z_{oh} and z_{oq} are the roughness lengths corresponding to transport of momentum, heat and moisture, respectively. The stability function for momentum is only a function of stability parameter ζ,

$$\psi_m(\zeta) = 2\ln\left(\frac{1+x}{2}\right) + \ln\left(\frac{1+x^2}{2}\right) - 2\tan^{-1}(x) + \pi/2; \;\; \zeta < 0 \tag{9}$$

$$\psi_m(\zeta) = -a_2\zeta; \;\; \zeta > 0, \tag{10}$$

where $x = (1 - a_1\zeta)^{1/4}$, $a_1 = 16$, $a_2 = 5$ and $\zeta \equiv z/L$ [*Businger*, 1966; *Businger et al.*, 1971; *Paulson*, 1970; *Dyer*, 1974; *Hogstrom*, 1988]. L is the Obukhov length scale defined as

$$L \equiv \frac{-u_*^3}{(\kappa g/\theta_v)\left(\overline{w'\theta'} + 0.61\theta\overline{w'q'}\right)}. \tag{11}$$

The stability functions for heat and moisture transfer are specified to be equal and are given by

$$\psi_h(\zeta) = \psi_q(\zeta) = 2\ln\left(\frac{1+x^2}{2}\right); \;\; \zeta < 0 \tag{12}$$

$$\psi_h(\zeta) = \psi_q(\zeta) = \psi_m; \;\; \zeta > 0. \tag{13}$$

[26] The set of equations are not closed without specification of the roughness lengths. A common parameterization for z_{om} over the sea is

$$z_{om} = \alpha u_*^2/g + 0.11\nu/u_*, \tag{14}$$

following *Charnock* [1955], *Smith* [1988], *Fairall et al.* [1996] and others, where α is the Charnock coefficient (typically $\alpha = 0.011$) and ν is the kinematic viscosity of dry air. The first term on the rhs of equation (14) states that the aerodynamic roughness of the surface is proportional to the downward turbulence momentum transport from the atmosphere. Numerous investigators have related variations in α to variations in wave state to include the larger wind stress observed over young growing waves and smaller wind stress observed over older, faster moving waves [*Donelan*, 1990; *Maat et al.*, 1991; *Smith et al.*, 1992; *Drennan et al.*, 2003]. For the bulk model without wave-state effects, we use the usual value of $\alpha = 0.011$. The second term on the rhs of equation (14) is the aerodynamically smooth flow (viscous) term [*Kondo*, 1975], which becomes important in the formulation when the wind stress is weak. As a result of this term, z_{om} is predicted to increase with decreasing u_* for u_* less than about 0.075 m s^{-1} (Figure 1).

[27] The roughness lengths for heat and moisture transport in the widely used COARE (Coupled Ocean Atmosphere Response Experiment) bulk flux algorithm [*Fairall et al.*, 1996] are specified as functions (f and g) of the dimensionless roughness Reynolds number R_r,

$$R_r \equiv (z_{om}u_*/\nu), \tag{15}$$

$$z_{oh} = f(R_r)\nu/u_*, \tag{16}$$

$$z_{oq} = g(R_r)\nu/u_*, \tag{17}$$

after *Liu et al.* [1979]. In contrast to z_{om}, the scalar roughness lengths are specified to decrease with increasing wind stress for $u_* > 0.2$ m s^{-1} (Figure 1). Sheltering by wave crests is thought to reduce scalar roughness with rougher seas.

[28] A gustiness velocity scale (w_g) is sometimes introduced in the bulk model to allow for non-zero fluxes with vanishing mean wind speed. In such case, the mean wind speed U in equations (3)–(5) is replaced by velocity $V = (U^2 + w_g)^{1/2}$ after *Godfrey and Beljaars* [1991]. For the data analyzed here, the bulk fluxes are not sensitive to use of w_g and we specify $w_g = 0$.

[29] Equations (3)–(17) enable an iterative solution for the fluxes based solely on the mean state quantities: U, θ, q and θ_s. Differences between individual 4-km average fluxes calculated from the LongEZ data and the bulk formulation described above (equations (3)–(17), Figure 1) and those calculated using the COARE algorithm version 2.5 are negligible. In COARE version 3.0 [*Fairall et al.*, 2003], the roughness lengths are slightly greater for wind speeds exceeding 10 m s^{-1}, thus slightly increasing the fluxes in strong winds, and the roughness lengths for heat and moisture are equated.

3.1. Roughness Lengths

[30] A possible cause of potential differences between the observed and bulk fluxes is that the stability functions are biased; however, these functions are thought to be better known than the roughness lengths, and are based on decades of tower-based measurements of the nondimensional gradient (mean vertical gradient normalized by the flux) (e.g., see the reviews in the works by *Hogstrom* [1988] and *Vickers and Mahrt* [1999]). The current data sets agree well with commonly used flux-variance similarity relationships for σ_w/u_*, σ_T/T_* and σ_q/q_* as a function of z/L, suggesting that atmospheric surface layer similarity applies. However, satisfying flux-variance similarity does not necessarily imply that the data satisfy flux-gradient similarity. Errors in the stability functions and the roughness lengths both probably contribute to differences between the observed and bulk fluxes, but it is not possible to separate the effects with the current aircraft data. We accept existing stability functions and focus on the roughness lengths.

[31] The roughness lengths that satisfy the bulk model can be calculated by substituting the observed fluxes into the bulk model and solving as

$$\ln(z_{om}) = \ln(z) - \kappa U u_*^{-1} - \psi_m, \tag{18}$$

$$\ln(z_{oh}) = \ln(z) - \kappa u_* (\theta_s - \theta)\left(\overline{w'\theta'}\right)^{-1} - \psi_h, \tag{19}$$

$$\ln(z_{oq}) = \ln(z) - \kappa u_* (q_s - q)\left(\overline{w'q'}\right)^{-1} - \psi_q. \tag{20}$$

The roughness lengths are sensitive to how they are averaged and how extreme values are handled [*DeCosmo et al.*, 1996; *Mahrt et al.*, 2003]. In this study, the logarithm of the roughness length is averaged. The frequency distribution of the log of the roughness length is approximately normal while the frequency distribution of the roughness length itself is strongly skewed. Averaging is better posed for normally distributed variables. A few extreme values of the roughness length outside the range 10^{-10} to 100 m were discarded from the averaging process.

[32] We note that relationships between the roughness lengths and the wind stress include self-correlation because the roughness lengths contain u_*. An apparent relationship between the roughness lengths and wind stress does not necessarily imply a physical relationship [*Andreas*, 2002; *Klipp and Mahrt*, 2004, and references therein]. Self-correlation causes z_{om} to increase with u_* and causes z_{oh} and z_{oq} to decrease with increasing u_* (equations (18)–(20)).

4. Bulk and Observed Fluxes

[33] Figures 2 and 3 and Table 1 compare bulk (section 3) and observed (section 2) fluxes. Some of the scatter in Figures 2 and 3 is presumably due to (1) random flux sampling errors, (2) flux divergence associated with advection below the measurement height, (3) non-equilibrium conditions due to flow over SST heterogeneity, and (4) wave-state effects.

4.1. Momentum

[34] The bulk model momentum fluxes are generally larger than the observed for the LongEZ data and smaller than observed for ASIT data. Consequently, the roughness length for momentum is larger based on the ASIT data compared to the aircraft data (Figure 4). This is consistent with *Edson et al.* [2004], who reported slightly smaller nondimensional wind shear (larger wind stress) than that given by the standard bulk formulation using the ASIT data. The scatter in the roughness lengths (not shown) is enormous, as found in most studies.

[35] The RMS difference between the observed and predicted fluxes is especially large for the aircraft-based momentum flux, where wind-wave interactions are more important compared to the sensible and latent heat fluxes. The bulk model has no independent information on wave state. In addition, random flux sampling errors are in general more severe for the momentum flux [*Vickers and Mahrt*, 1997]. The momentum fluxes from the tower have less scatter compared to the aircraft data partly owing to the reduction in random sampling errors associated with the 1-hour averaging time at the tower compared to 4-km averaging for the aircraft. However, the small amount of scatter and bias for the ASIT data is surprising given exclusion of wave-state effects.

[36] The dependence of z_{om} on u_*^2 g^{-1} for the current aircraft data sets (Figure 4) is similar to the relationship found by *Mahrt et al.* [2003, Figure 1] using offshore tower and buoy data from six different field programs. In that study and the current study, the observed momentum roughness length is less than predicted for weak to moderate wind stress and approximately equal to the prediction for strong wind stress. This would be consistent with greater flux loss due to flux divergence in weaker winds. We have attempted to correct for flux divergence below the aircraft level (section 2.5); however, the correction may be inadequate in very weak wind conditions.

[37] In near-collapsed turbulence, defined as $u_* < 0.05$ m s^{-1}, the bulk momentum flux exceeds the observed momentum flux by a factor of 10 for LongEZ CBLAST data,

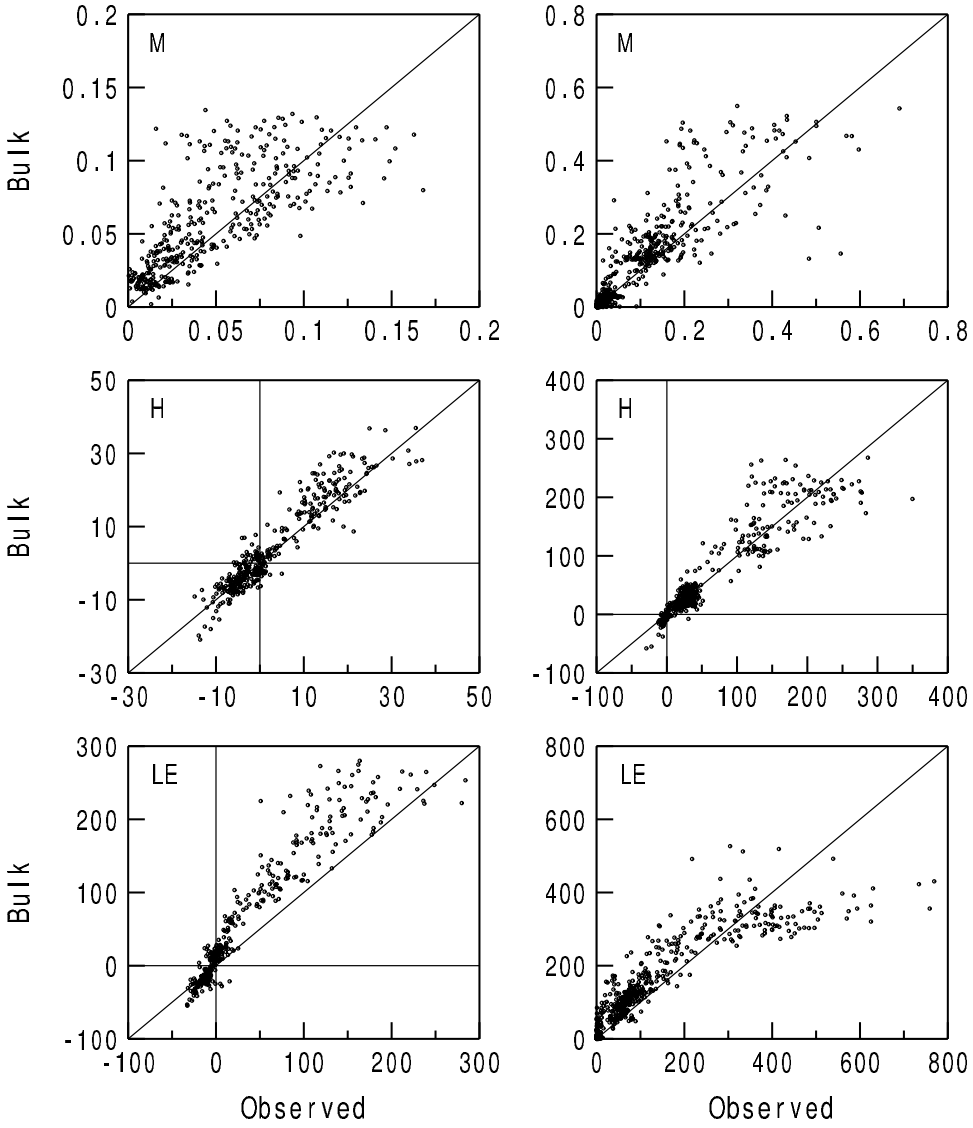

Figure 2. Bulk fluxes of momentum (M) (N m^{-2}), sensible heat (H) (W m^{-2}), and latent heat (LE) (W m^{-2}) as a function of the observed fluxes with $\lambda = 4$ km averaging for LongEZ CBLAST (left column) and SHOWEX (right column) data.

a factor of 3 for LongEZ SHOWEX data and a factor of 2 for the ASIT data. In contrast to many studies, this suggests that the modeled drag coefficient is too large in very weak turbulence conditions. The bulk model generally fails to predict these near-collapsed cases observed by both the tower and the aircraft possibly in part owing to wave-state effects not included in the model. For example, the wind stress is reduced relative to the bulk prediction for conditions with weak wind following swell [*Phillips and Banner*, 1974; *Smedman et al.*, 1994; *Mitsuyasu and Kusaba*, 1996; *Grachev and Fairall*, 2001].

[38] Possibly because of self-correlation, we do not find any evidence from the aircraft data for a smooth flow regime where z_{om} increases with decreasing u_* for small u_*. The ASIT data hint at the existence of a smooth flow regime (Figure 4). *Andreas et al.* [2004] found no evidence of a smooth flow regime from their analysis of SHEBA (Surface Heat Budget of the Arctic Ocean) and ISW (Ice Station Weddell) data collected over snow surfaces. *Mahrt et al.* [2003] also found no evidence of a smooth flow regime in their estimates of z_{om} based on data from offshore towers and buoys.

[39] The lack of a smooth flow regime is slightly sensitive to the flux calculation method. Use of conventional averaging times of 10 to 30 minutes for τ (section 2.4) in very weak turbulence often inadvertently includes mesoscale motions in the calculated flux. These mesoscale fluxes can be larger than the turbulence flux and are typically random and unrelated to the local wind shear or stratification [*Vickers and Mahrt*, 2006]. Such primarily random wind stress components (positive or negative) are converted to positive bias when u_* is calculated from the stress components. We speculate that some previous studies that found evidence of a smooth flow regime may have been partially influenced by this bias.

4.2. Sensible Heat

[40] Good general agreement is found between modeled and observed sensible heat flux. However, inspection of the roughness lengths (Figure 4) shows that the good agreement

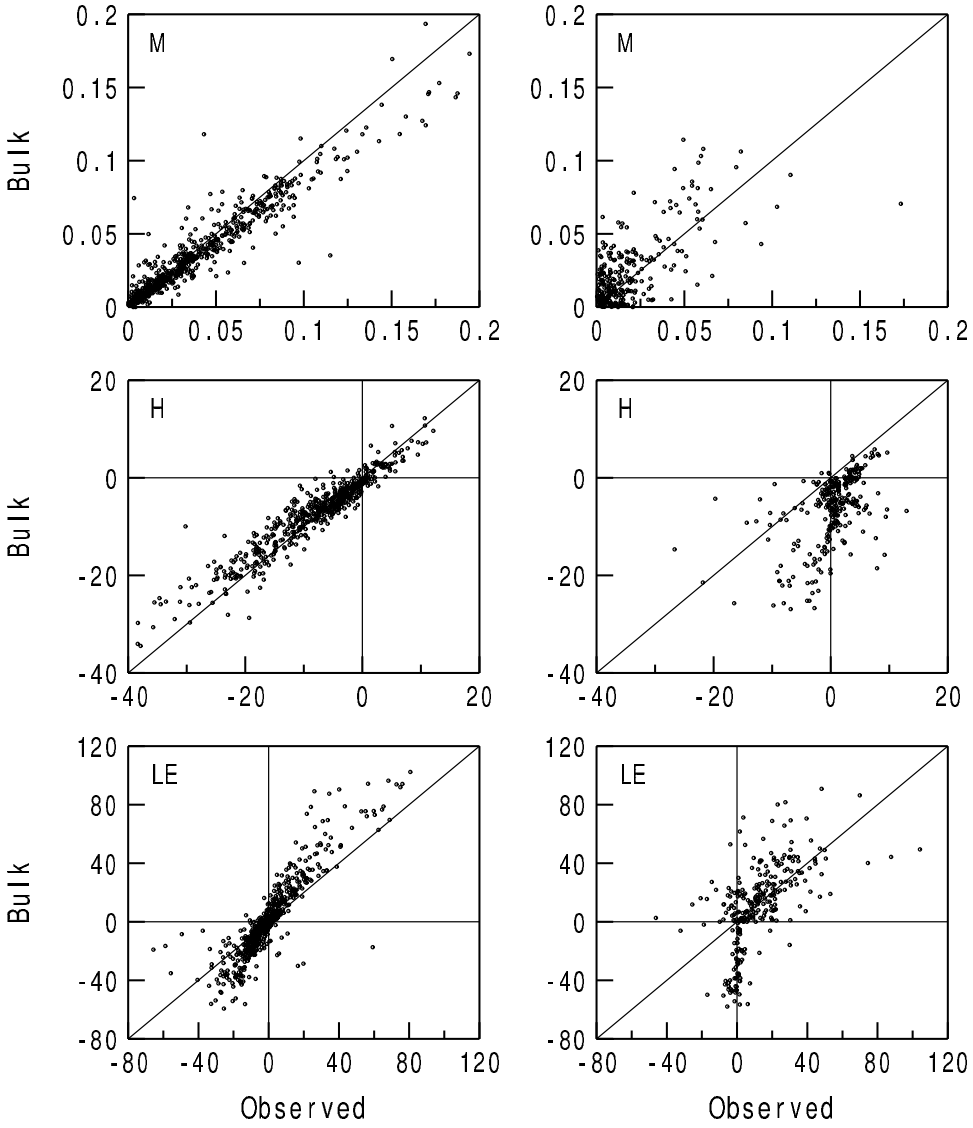

Figure 3. Same as Figure 2 but for ASIT CBLAST data (left column) and Pelican CBLAST (right column) data.

for weak to moderate turbulence conditions in the LongEZ data is due to cancellation of two errors, where z_{om} is overpredicted and z_{oh} is underpredicted, with the result that C_h (equation (7)) agrees reasonably well with the observations. The aircraft data indicate that z_{oh} decreases with increasing wind stress, as predicted by the bulk model, while z_{oh} from ASIT has no clear relationship with wind stress. On average, the downward sensible heat flux from ASIT is larger than the bulk model prediction.

4.3. Latent Heat

[41] The magnitude of the bulk latent heat flux clearly exceeds the observed for LE < 300 W m^{-2} for both the aircraft and tower data; however, for the largest LE > 300 W m^{-2} observed during SHOWEX, the bulk latent heat flux is less than the observed. *Vickers and Esbensen* [1998] generally found that the COARE model latent heat fluxes were larger than the observed fluxes based on comparisons with eddy-correlation fluxes calculated using NCAR Electra aircraft measurements in the COARE experiment. This general result is consistent with the present analysis. Excluding for the moment the periods with the largest LE and the strongest wind speeds observed by the aircraft in SHOWEX, the observed z_{oq} is significantly smaller than specified in the bulk model for both the aircraft and tower data sets (Figure 4). Larger modeled latent heat flux compared to

Table 1. Correlation Coefficients Between Observed and Bulk Fluxes for a Range of Flux Averaging Length Scales (λ) for the LongEZ Data in CBLAST and SHOWEX[a]

Data Set	Flux	2 km	4 km	8 km	16 km	32 km
CBLAST	M	0.72	0.74	0.78	0.81	0.80
	H	0.93	0.94	0.95	0.97	0.99
	LE	0.94	0.94	0.96	0.97	0.99
SHOWEX	M	0.84	0.87	0.92	0.96	0.98
	H	0.92	0.94	0.96	0.98	0.98
	LE	0.86	0.88	0.90	0.92	0.92

[a]M, momentum; H, sensible heat; LE, latent heat.

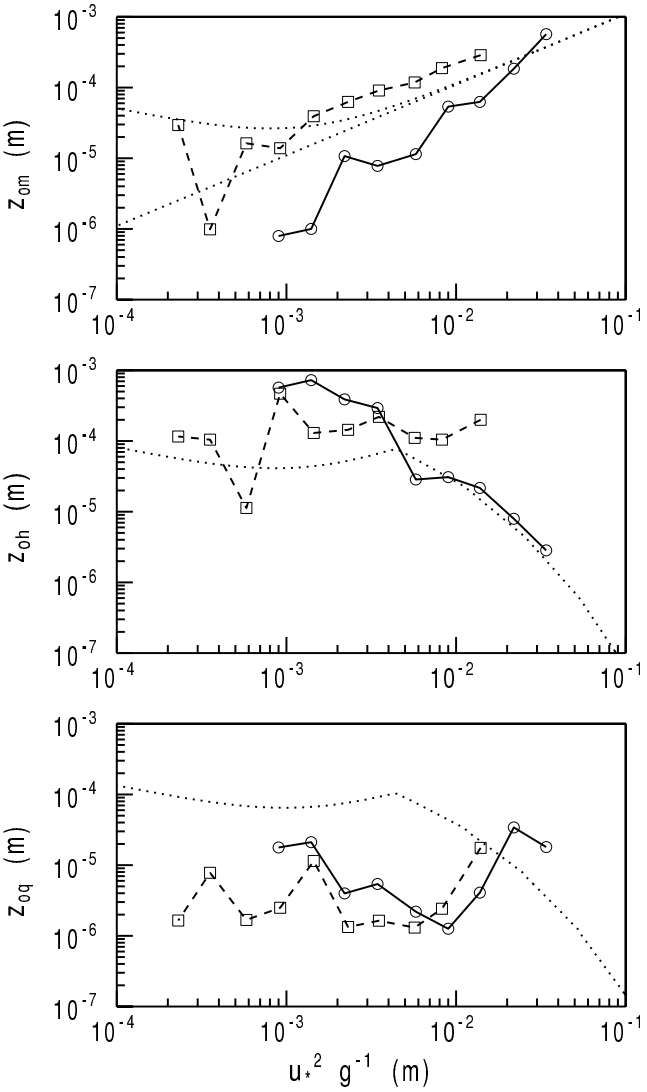

Figure 4. Bin-averaged roughness lengths (meters) for combined LongEZ CBLAST and SHOWEX data as a function of $u_*^2\ g^{-1}$ (meters). Dotted curves are the bulk model (equations (14)–(17)). Dotted straight line is the z_{om} rough flow term only. ASIT data are denoted by the dashed curves with squares.

observed for all the data sets is not sensitive to the flux calculation method.

5. Scalar Roughness Ratio

[42] In contrast to the bulk model formulation, where the roughness lengths for heat and moisture transport are specified to be equal, both the aircraft and tower data indicate that the scalar roughness length ratio (z_{oh}/z_{oq}) is significantly greater than unity with the exception of the strongest wind-speed cases (discussed below). The result that $z_{oh} > z_{oq}$ is consistent with other observational evidence that the dimensionless variance of moisture tends to be larger than that of temperature, or equivalently, that R_{wT} exceeds R_{wq}, where R is the correlation coefficient [*Katul and Hsieh*, 1999; *Asanuma and Brutsaert*, 1999; *DeBruin et al.*, 1999]. The more efficient transport of heat for these data

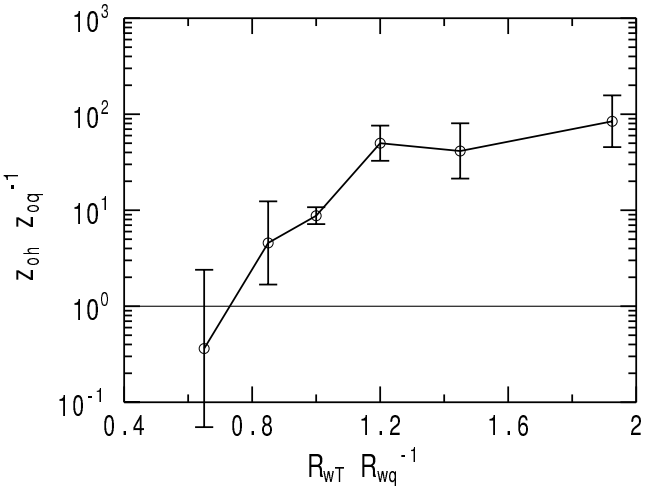

Figure 5. Observed 4-km scalar roughness length ratio (z_{oh} divided by z_{oq}) as a function of the transport efficiency ratio (R_{wT} divided by R_{wq}) for combined LongEZ CBLAST and SHOWEX data.

could be associated with the domination of buoyancy generation of turbulence by temperature fluctuations instead of moisture fluctuations. In this sense, moisture acts more like a passive scalar than does temperature. The current data sets indicate that the scalar roughness length ratio is strongly coupled to the transport efficiency ratio (Figure 5).

[43] *DeBruin et al.* [1999] suggested that differences between entrainment of heat and moisture at the top of the boundary layer could contribute to differences in transport efficiency. This influence is difficult to access with the current data. *Andreas et al.* [1998] and others have suggested that micro-scale surface moisture heterogeneity contributes to differences between R_{wT} and R_{wq} over land surfaces. Over the ocean, these influences are expected to be negligible.

[44] In the strongest observed winds, the scalar roughness length ratio (Figure 6) becomes less than unity owing to the

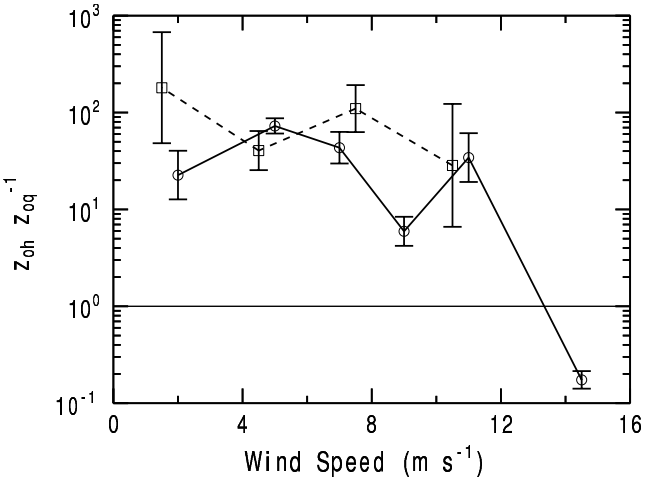

Figure 6. Observed 4-km scalar roughness length ratio (z_{oh} divided by z_{oq}) as a function of the 10-m wind speed (m s^{-1}) for combined LongEZ CBLAST and SHOWEX data. ASIT data are denoted by the dashed curve with squares.

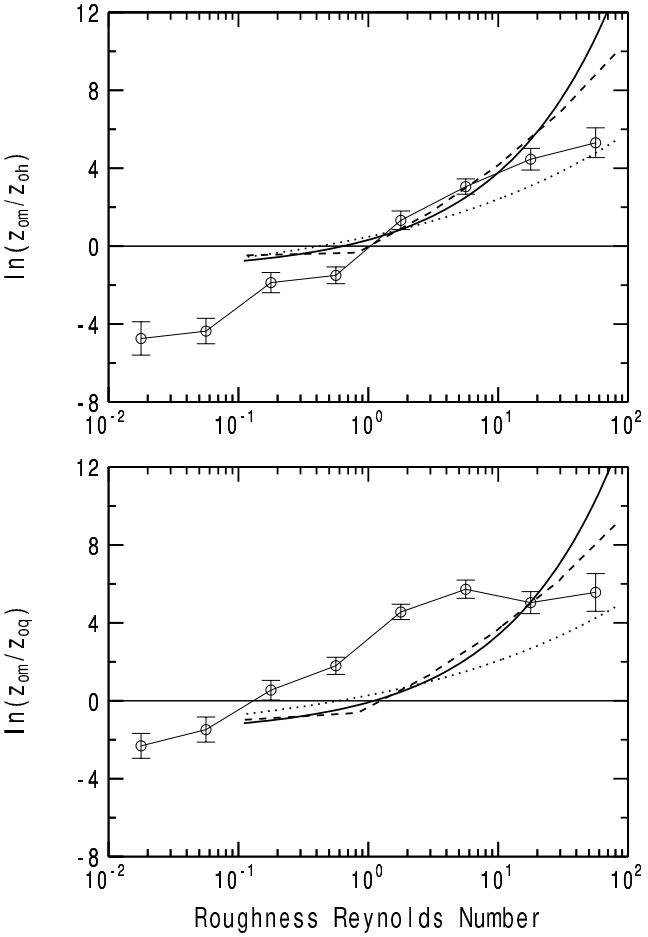

Figure 7. Observed roughness length ratio z_{om} divided by (top) z_{oh} and (bottom) z_{oq} as a function of roughness Reynolds number for combined LongEZ CBLAST and SHOWEX data (circles with error bars). The solid curve is from *Zilitinkevich et al.* [2001], dashed curve is from *Liu et al.* [1979], and dotted curve is from *Brutsaert* [1982].

combination of a precipitous decrease in z_{oh} coupled with a large increase in z_{oq} (Figure 4). The decrease in z_{oh} could be due to wave sheltering [*Liu et al.*, 1979], while the increase in z_{oq} could be related to wave breaking. *Donelan* [1990] postulated that at high wind speeds the decrease in moisture flux due to sheltering may be offset by an increase due to a disruption of the surface microlayer by breaking waves. The observations here indicate no clear dependence of the scalar roughness length ratio on wind speed until a threshold wind speed (about 12 m s^{-1}) is reached, wherein the ratio plummets by a factor of nearly 200. This behavior is consistent with a threshold wind speed required for initiation of wave breaking.

[45] The majority of the data indicating enhanced moisture transport ($z_{oq} > z_{oh}$) occur on 30 November in SHOWEX, with isolated cases also occurring on 16 and 28 November. All three of these days are characterized by breaking waves and cold, dry air advection from land located 50 km or more to the northwest of the study area. These are large-scale cold air outbreaks leading to strong instability and roll circulations. Roll vortices were inferred from data analysis and satellite images on 16 November, when the aircraft measured latent heat fluxes in excess of 500 W m^{-2}.

[46] Previous studies by *Andreas and Monahan* [2000] and *DeCosmo et al.* [1996] did not find enhanced moisture transport over breaking waves and proposed that the cause was rapid saturation of the near-surface air which reduces further moisture transport. However, for these three days in SHOWEX, a strong supply of cold dry air is available due to advection from land. We speculate that the occurrence of enhanced moisture flux ($z_{oq} > z_{oh}$) over breaking waves may be confined to coastal regions with strong offshore advection of dry air; however, the erratic behavior of the bin-averaged z_{oq} from both the tower and aircraft data suggests that we need more data to make more definitive conclusions. In addition, organization of the turbulence by the roll circulations [*LeMone*, 1976] probably leads to large spatial variability of the turbulence flux and cross-wind flight tracks would be more useful.

[47] The observed roughness lengths are contrasted with previously published formulations in Figure 7 using the same variables as *Zilitinkevich et al.* [2001, Figure 2]. The major difference is that this study finds large observed values of z_{om} divided by z_{oq} for roughness Reynolds number between 0.3 and 10.

6. SST Variability

[48] We now examine the influence of SST variability on the mean flow, the fluxes and the flux-gradient relationship. What scales and amplitudes of SST variability need to be resolved in a model in order to capture the significant variability in the air-sea fluxes?

[49] For the data sets considered here, flux variations along a flight segment are dominated by variations in SST, as in Figure 8 showing the response of the air-sea fluxes to a 10-km-wide cold pool. The sensible heat flux is highly correlated with SST with a 1- to 2-km downstream spatial lag at the aircraft level. Over the warm water downstream of the cold pool, large variations in latent heat flux occur that are not related to the SST or to the low-level wind speed or humidity (not shown). The LE variations could be related to changes in entrainment at the top of the boundary layer.

[50] To evaluate the dependence of fluxes on SST variations, the relative variation is examined for 16-km flight segments in the CBLAST pilot experiment. A sequence of τ-scale averages (section 2.4) are used to compute the flight segment mean and standard deviation of the fluxes and the SST. The τ-scale averaging eliminates SST variability on length scales comparable to and smaller than the turbulence scales. Because the relative variation, defined as the standard deviation divided by the mean, is not well posed when the mean flux vanishes, a few 16-km segments are excluded from the analysis.

[51] Variations in the sensible heat flux are most strongly related to variations in SST, while the momentum flux and moisture flux are less related (Figure 9). Extrapolating the linear relationships in Figure 9 to zero SST variability yields an estimate of the flux variability that is present for spatially homogeneous SST. Such estimates are 25, 13 and 20% for M, H and LE, respectively. These estimates include random

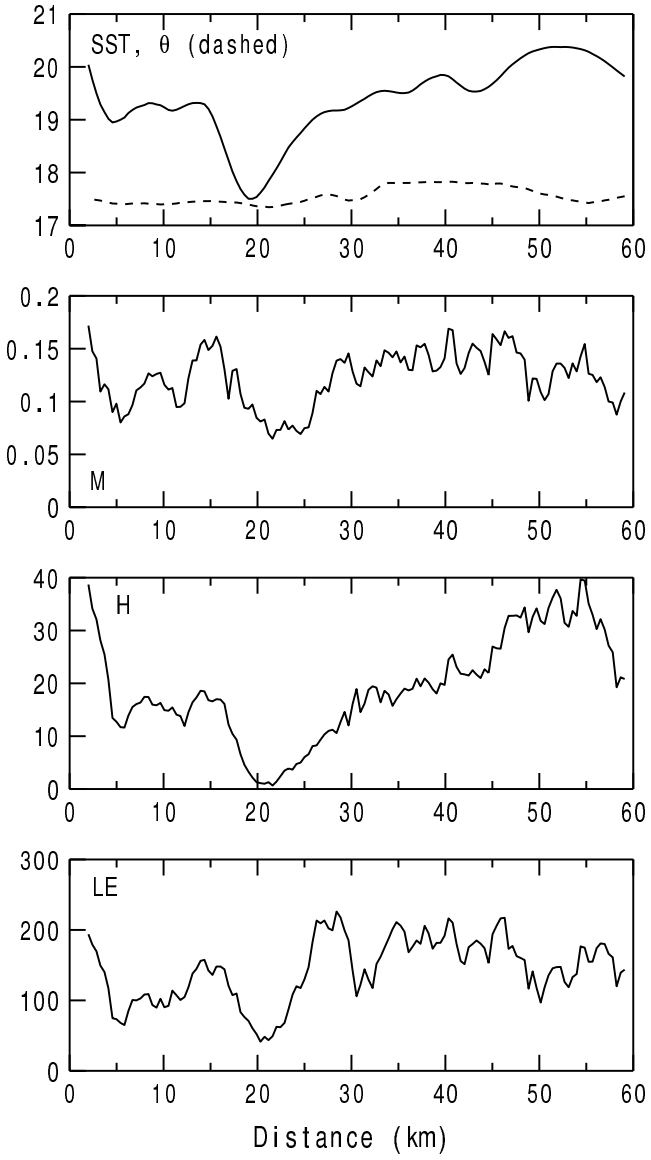

Figure 8. Spatial variation of SST and 10-m θ (C), momentum flux (M) (N m^{-2}), sensible heat flux (H) (W m^{-2}), and latent heat flux (LE) (W m^{-2}) for a single flight segment on 27 July in the CBLAST pilot experiment. Mean flow is left to right.

flux sampling errors and influences of variations in wave state and mean atmospheric quantities.

6.1. Averaging Length Scale

[52] For spatially homogeneous conditions, the random flux sampling error decreases with increasing averaging length λ due to capturing an increasing number of samples of the transporting eddies. On the other hand, the bulk model may break down with increasing λ owing to capture of significant heterogeneity. For example, consider a sharp SST front that generates strong upward heat flux over a small fraction of the flight track or model grid box that includes warm water, while over the majority of the track, the heat flux is weakly downward over cool water. The bulk gradient ($\theta_s - \theta$) averaged over the flight track can be negative, yet the average heat flux can be positive (Figure 10), leading to a negative exchange coefficient for heat in terms of the flight track or model grid box averaged quantities. This situation occurs in part because the exchange coefficients are stability dependent, and therefore the response of the heat flux to changes in U ($\theta_s - \theta$) is nonlinear. This case is discussed further by *Mahrt et al.* [2004].

[53] The example in Figure 10 represents an extreme case of sharp heterogeneity where increasing λ leads to a breakdown of the bulk model. However, on average for all the current data, the effect of decreased random flux sampling error appears to be larger than the influence of increased captured heterogeneity. As a result, the agreement between bulk and observed fluxes generally improves with increasing λ even with surface heterogeneity (Table 1). The

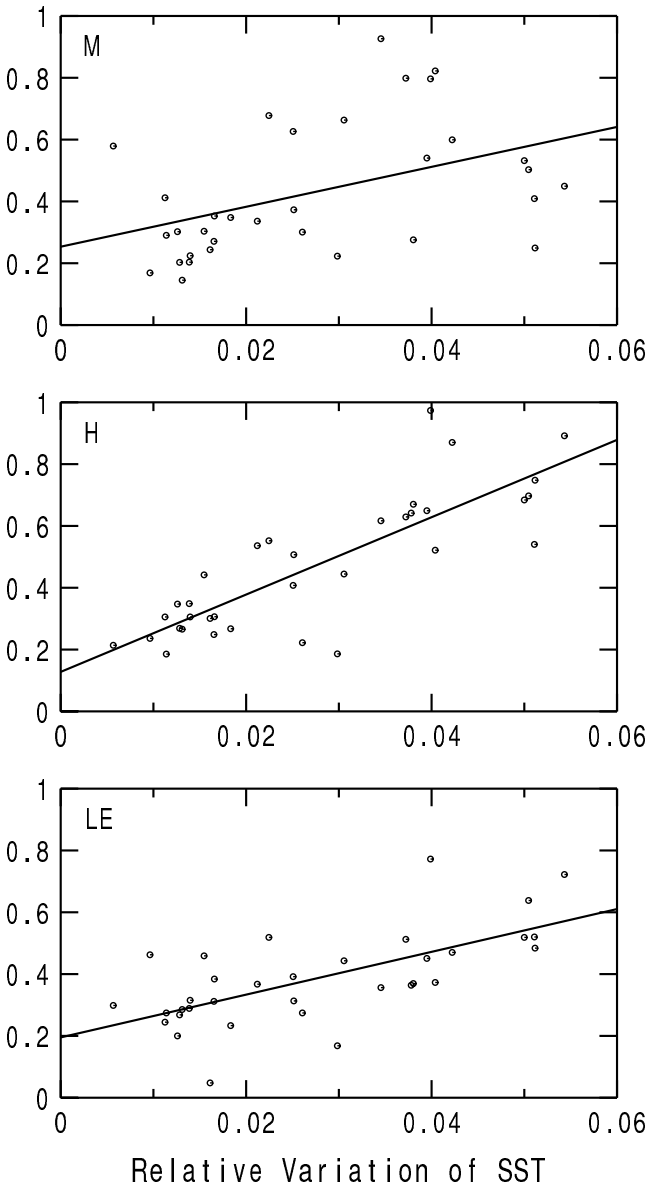

Figure 9. Relative variation of the momentum flux (M), sensible heat flux (H), and latent heat flux (LE) as a function of the relative variation in SST in the CBLAST pilot experiment.

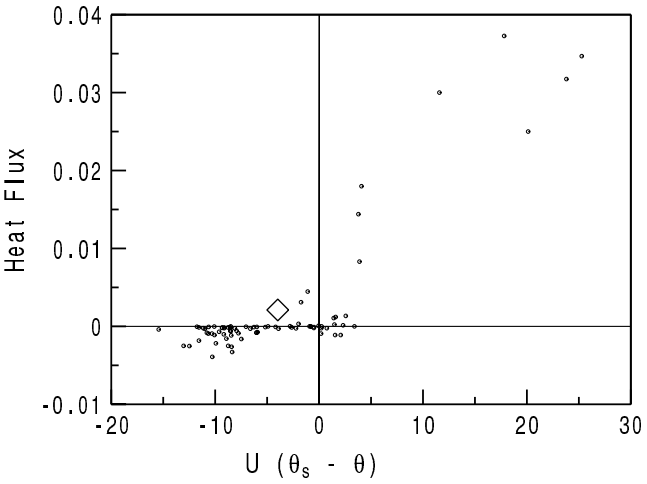

Figure 10. Kinematic heat flux (C m s^{-1}) as a function of U ($\theta_s - \theta$) for $\lambda = 4$ km averaging near the edge of the Gulf stream on 20 November in SHOWEX. The diamond is from spatial averages over the 20-km flight track.

improvement with increasing averaging length scale highlights sampling problems which are often a major difficulty with aircraft data without a large number of passes over the same flight track in similar mean flow conditions.

6.2. Amplitude of Response

[54] Discontinuities in SST (fronts) are identified using the Haar transform, which calculates the difference in SST over two adjacent 4-km half-window means. A large positive (negative) value of the transform indicates an increase (decrease) in SST in the downwind direction which is coherent on the scale of the 8-km window. The horizontal structure upstream and downstream from the changes in SST is composited on the basis of the value of the transform to examine the average response of the fluxes and mean flow to the amplitude of the SST change.

[55] The momentum, sensible heat and latent heat fluxes and the vertical velocity variance change by 25 to 50% when the 8-km SST transform exceeds 1 C (Figure 11), equivalent to an SST gradient of 0.25 C km^{-1} with 4-km resolution grid boxes. When the SST gradient is less than this value at this spatial scale, the response of the fluxes and the mean flow to the SST change is of questionable significance. The change in the fluxes is similar in magnitude and opposite in sign for flow over cold-to-warm and warm-to-cold changes in SST. There is a small yet systematic response of the low-level mean wind speed and air temperature to SST transforms exceeding 1 C (Figure 11). As the flow moves from colder to warmer water, the mean flow at 10 m warms, moistens, accelerates and becomes more turbulent, while the opposite is true for flow from warm to cold water. There is larger scatter in the low-level mean wind speed adjustment in flow from warm to cooler water.

6.3. Low-Level Flow Acceleration

[56] A case of flow from cool to warm water documented by three low-level repeat passes and four repeat slant soundings over each end of the flight track is shown in Figure 12. The mean wind direction was relatively steady from the east (open ocean) with 10-m wind speeds ranging from 6 to 8 m s^{-1} along the track. The bulk temperature difference ($\theta_s - \theta$) increased nearly 3 C in the downstream direction over the 18-km track owing to an increase of SST toward the west. On the basis of very limited observations, we speculate that the SST was even cooler farther upstream of the flight track. The only significant time dependence found was for the mean air temperature profile over the cool end of the track, where the temperature was increasing slightly with time.

[57] Over the cool end of the track, the stratification and wind shear were strong and the turbulence kinetic energy was very small. Shear generation of turbulence was strongly suppressed by the stratification. On the basis of the decrease of TKE with height, the boundary layer depth over the cool water was only about 50 m. Over the warm end of the track, the potential temperature was nearly constant with height, the mean wind shear was significantly reduced and the boundary layer depth was estimated to be well above the highest measurement level.

[58] Over the cool water, the flow above the shallow stable boundary layer partially decouples from the surface drag and accelerates, while within the stable boundary layer, strong vertical stress divergence due, in part, to the shallow boundary layer depth decelerates the near-surface mean flow. Large wind shear results. Downwind over the warmer water, surface heating deepens the boundary layer and the decoupled flow aloft now entrains into the boundary layer, couples with the surface drag and decelerates. At low levels, the flow accelerates over the warm water due to weaker stress divergence associated with deeper boundary layer depth. The relative increase in the surface stress over the warm end of the track is less than the relative increase in boundary layer depth, and thus the vertical stress divergence decreases downstream, which contributes to acceleration of the mean flow. The thermally induced horizontal pressure gradient due to the change in the low-level air temperature is thought to be a secondary effect (E. D. Skyllingstad et al., Effects of mesoscale sea-surface temperature fronts on the marine boundary layer, submitted to *Boundary Layer Meteorology*, 2006).

7. Conclusions

[59] A bulk flux model with no wave-state information, similar to that used to parameterize air-sea fluxes in most large-scale atmospheric models, was evaluated using aircraft and tower eddy-correlation data collected off the northeast coast of the United States in summer and winter. While we cannot rule out the possibility that the measurements underestimate surface fluxes, the systematic differences between bulk and observed latent heat fluxes appear to be too large to be fully explained by measurement problems. Model predictions of the sensible heat and momentum fluxes were reasonable within the data uncertainties; however, the reasonable agreement for the sensible heat flux was due to cancellation of two errors, where z_{om} was overpredicted and z_{oh} was underpredicted.

[60] With weak to moderate winds, the observed fluxes of latent heat were systematically smaller than predicted by the model. The more efficient transfer of heat compared to

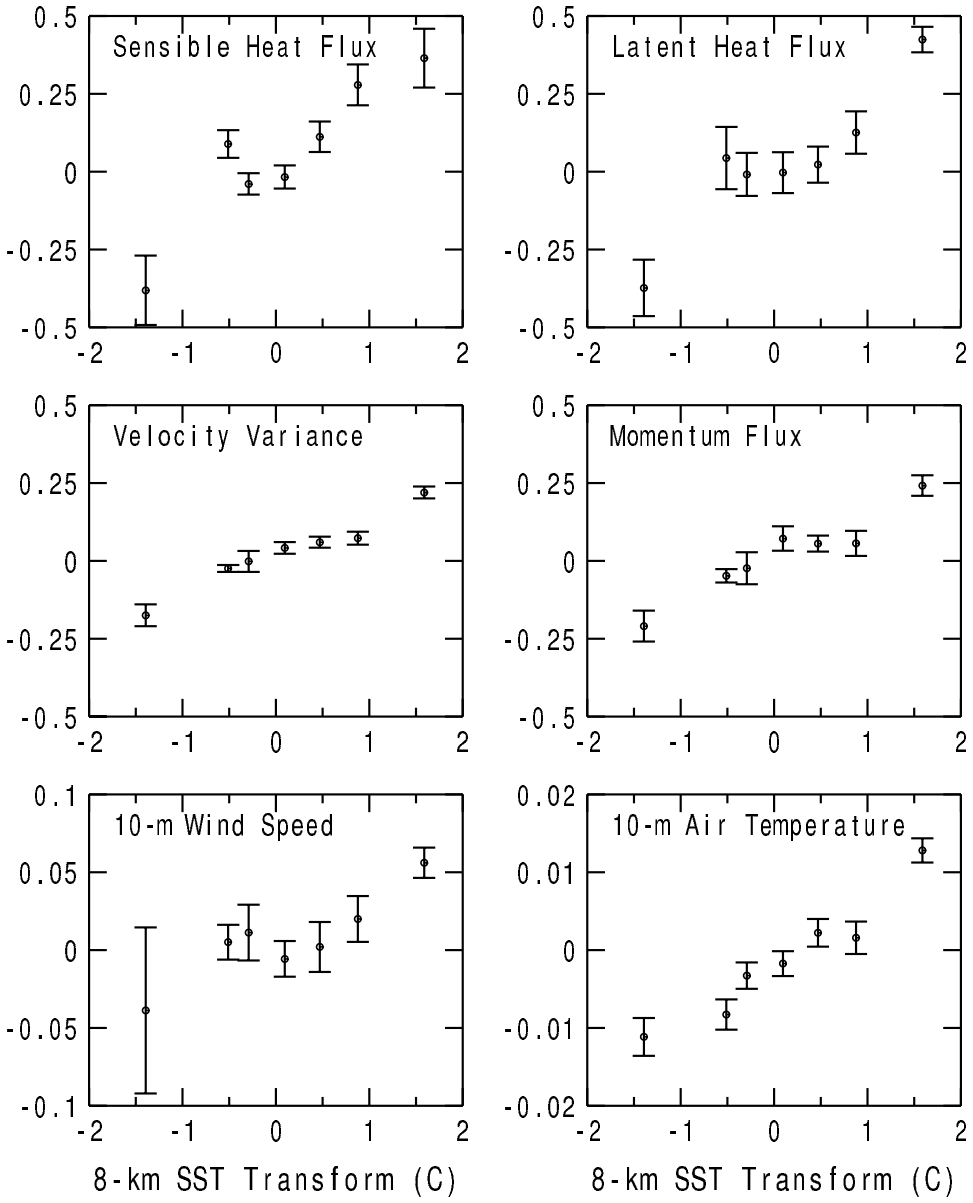

Figure 11. Mean and standard error of the relative change (downstream minus upstream divided by the mean) in the fluxes, vertical velocity variance, and mean fields as a function of the SST Haar transform (C). Each bin contains an equal number of samples. Data are from the LongEZ CBLAST pilot experiment.

moisture for weak to moderate winds is consistent with the greater importance of temperature, as compared to moisture, in the buoyancy generation of turbulence in these data sets. The scalar roughness length ratio (z_{oh}/z_{oq}) is of order 50 except for the strongest wind-speed conditions associated with wave breaking, where it decreases to order 0.1. The enhanced moisture flux over breaking waves is coincident with a large-scale cold air outbreak from the continent.

[61] The tower-based momentum fluxes were slightly larger than predicted with small scatter, while the aircraft-based momentum fluxes were systematically smaller than predicted with large scatter. Inclusion of wave-state effects in the bulk formulation may be required to better predict variations in the momentum flux. In particular, the bulk model overpredicts the momentum flux for cases of moderate winds but very weak wind stress possibly due to wind following swell conditions.

[62] The comparison between bulk and observed fluxes from the aircraft data improves with increasing flux averaging scale over the range of scales tested (2 to 32 km) even with surface heterogeneity. This implies that the reduction in random flux sampling errors owing to increasing averaging scale more than offsets the problems with the flux-gradient relationship with increasing scale owing to capturing additional spatial heterogeneity. In extreme cases where the flight track includes a large-amplitude SST front, the bulk model breaks down and fails to capture the correct sign of the spatially averaged heat flux, in part owing to the nonlinear response of the heat flux to the bulk gradient. However, more typical SST variability does not seriously

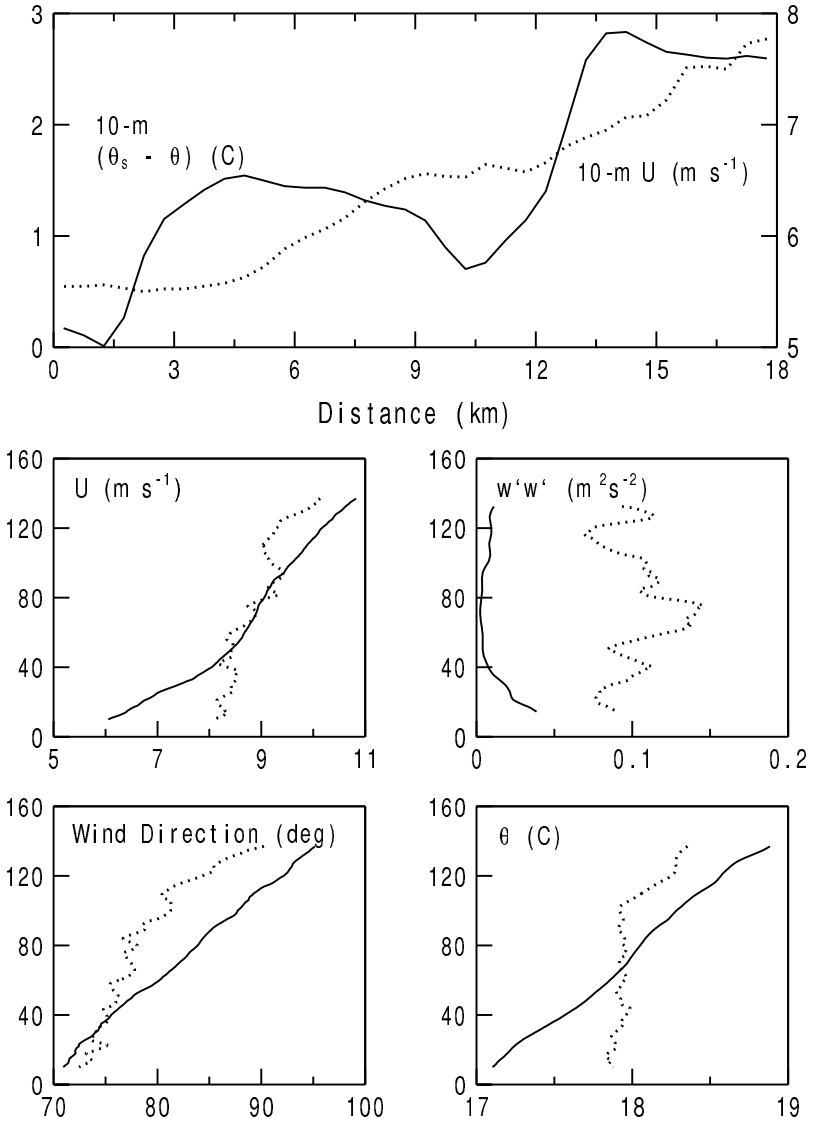

Figure 12. Composite mean horizontal (top panel) and vertical (bottom four panels) structure on 30 July in the CBLAST pilot experiment. For the vertical profiles (y-axis = altitude in meters), solid (dotted) curves are composites over the cold (warm) end of flight track. In top panel, mean flow is left to right, from cool to warmer water.

degrade the performance of the bulk model for predicting area-averaged fluxes.

[63] The momentum, sensible heat and latent heat fluxes respond strongly to SST changes which exceed 1 C in amplitude on the 8-km scale (a 1 C change between two adjacent 4-km averages of SST). When the change in SST is less than this value, the response of the fluxes, at least as measured by the aircraft, is not significant. A larger number of repeat passes over the same SST feature would be required to extend this analysis to shorter scales. A case study of flow from cold to warm water shows that acceleration of the low-level mean wind over the warm pool appears to be related to the decrease in vertical stress divergence associated with a much deeper boundary layer over the warm water.

[64] **Acknowledgments.** The authors thank Jim Edson for directing the CBLAST Weak Wind experiment and collecting the ASIT data, the late Tim Crawford for the LongEZ data, and Djamal Khelif and Haf Jonsson for collecting the Pelican data. This material is based on work supported by the Marine Meteorology Program of the Office of Naval Research under grants N00014-01-1-0029, N00014-01-1-0084, and N00014-05-1-0032.

References

Andreas, E. L. (2002), Parameterizing scalar transfer over snow and ice: A review, *J. Hydrometeorol.*, *3*, 417–432.

Andreas, E. L., and E. C. Monahan (2000), The role of whitecap bubbles in air-sea heat and moisture exchange, *J. Phys. Oceanogr.*, *30*, 433–442.

Andreas, E. L., R. J. Hill, J. R. Gosz, D. I. Moore, W. D. Otto, and A. D. Sarma (1998), Statistics of surface-layer turbulence over terrain with metre-scale heterogeneity, *Boundary Layer Meteorol.*, *86*, 379–408.

Andreas, E. L., R. E. Jordan, P. S. Guest, O. G. Perrson, A. A. Grachev, and C. W. Fairall (2004), Roughness lengths over snow, paper presented at 18th Conference on Hydrology, Am. Meteorol. Soc., Boston, Mass.

Asanuma, J., and W. Brutsaert (1999), The effect of chessboard variability of the surface fluxes on the aggregated turbulence fields in a convective atmospheric surface layer, *Boundary Layer Meteorol.*, *91*, 37–50.

Brutsaert, W. (1982), *Evaporation into the Atmosphere—Theory, History and Applications*, 299 pp., Springer, New York.

Businger, J. A. (1966), Transfer of momentum and heat in the planetary boundary layer, paper presented at Symposium on Arctic Heat Budget and Atmospheric Circulation, RAND Corp., Santa Monica, Calif.

Businger, J. A., J. C. Wyngaard, Y. Izumi, and E. F. Bradley (1971), Flux profile relationships in the atmospheric surface layer, *J. Atmos. Sci.*, *28*, 181–189.

Charnock, H. (1955), Wind stress on a water surface, *Q. J. R. Meteorol. Soc.*, *81*, 639–640.

Crescenti, G. H., T. L. Crawford, and E. J. Dumas (1999), Data Report: LongEZ (N3R) Participation in the 1999 Shoaling Waves Experiment (SHOWEX)—Spring pilot study, *NOAA Tech. Memo. ERl ARL-232*, 86 pp., Natl. Oceanic and Atmos. Admin., Silver Spring, Md.

DeBruin, H. B., B. van Den Hurk, and L. Kroon (1999), On the temperature-humidity correlation and similarity, *Boundary Layer Meteorol.*, *93*, 453–468.

DeCosmo, J., K. B. Katsaros, S. D. Smith, R. Anderson, W. A. Oost, K. Bumke, and H. Chadwick (1996), Air-sea exchange of water vapor and sensible heat: The Humidity Exchange Over the Sea (HEXOS) results, *J. Geophys. Res.*, *101*, 12,001–12,016.

Donelan, M. A. (1990), Air-sea interaction, in *Ocean Engineering Science*, edited by B. LeMehaute and D. M. Hanes, pp. 239–292, John Wiley, Hoboken, N. J.

Drennan, W. M., H. Graber, D. Hauser, and C. Quentin (2003), On the wave age dependence of wind stress over pure wind seas, *J. Geophys. Res.*, *108*(C3), 8062, doi:10.1029/2000JC000715.

Dyer, A. J. (1974), A review of flux-profile relationships, *Boundary Layer Meteorol.*, *7*, 363–372.

Edson, J. B., and C. W. Fairall (1998), Similarity relationships in the marine atmospheric surface layer for terms in the TKE and scalar variance budgets, *J. Atmos. Sci.*, *55*, 2311–2328.

Edson, J. B., R. Crofoot, W. McGillis, and C. Zappa (2004), Investigations of flux-profile relationships in the marine atmospheric boundary layer during CBLAST, paper presented at 16th Symposium on Boundary Layers and Turbulence, Am. Meteorol. Soc., Portland, Maine.

Fairall, C. W., E. F. Bradley, D. P. Rogers, J. B. Edson, and G. S. Young (1996), Bulk parameterization of air-sea fluxes for Tropical Ocean-Global Atmosphere Coupled Ocean Atmosphere Response Experiment, *J. Geophys. Res.*, *101*, 3747–3764.

Fairall, C. W., E. F. Bradley, J. E. Hare, A. Grachev, and J. B. Edson (2003), Bulk parameterization of air-sea fluxes: Updates and verification for the COARE algorithm, *J. Clim.*, *16*, 571–591.

Godfrey, J. S., and A. C. M. Beljaars (1991), On the turbulent fluxes of buoyancy, heat, and moisture at the air-sea interface at low wind speeds, *J. Geophys. Res.*, *96*, 22,043–22,048.

Grachev, A., and C. W. Fairall (2001), Upward momentum transfer in the marine boundary layer, *J. Phys. Oceanogr.*, *31*, 1698–1711.

Hare, J. E., T. Hara, J. B. Edson, and J. M. Wilczak (1997), A similarity analysis of the structure of airflow over surface waves, *J. Phys. Oceanogr.*, *27*, 1018–1037.

Hogstrom, U. (1988), Non-dimensional wind and temperature profiles in the atmospheric surface layer: A re-evaluation, *Boundary Layer Meteorol.*, *42*, 55–78.

Howell, J. F., and J. Sun (1999), Surface-layer fluxes in stable conditions, *Boundary Layer Meteorol.*, *90*, 495–520.

Katul, G. G., and C. I. Hsieh (1999), A note on the flux-variance similarity relationships for heat and water vapour in the unstable atmospheric surface layer, *Boundary Layer Meteorol.*, *90*, 327–338.

Khelif, D., H. Jonsson, and C. A. Friehe (2004), Turbulence measurements from aircraft during CBLAST-Low, *Eos Trans. AGU*, *84*(52), Ocean Sci. Meet. Suppl., Abstract OS32A-07.

Klipp, C., and L. Mahrt (2004), Flux-gradient relationship, self-correlation and intermittency in the stable boundary layer, *Q. J. R. Meteorol. Soc.*, *130*, 2087–2103.

Kondo, J. (1975), Air-sea bulk transfer coefficients in diabatic conditions, *Boundary Layer Meteorol.*, *9*, 91–112.

LeMone, M. A. (1976), Modulation of turbulence energy by longitudinal rolls in an unstable planetary boundary layer, *J. Atmos. Sci.*, *33*, 1308–1320.

Liu, W. T., K. B. Katsaros, and J. A. Businger (1979), Bulk parameterization of the air-sea exchange of heat and water vapor including the molecular constraints at the interface, *J. Atmos. Sci.*, *36*, 1722–1735.

Maat, N., C. Kraan, and W. A. Oost (1991), The roughness of wind waves, *Boundary Layer Meteorol.*, *54*, 89–103.

Mahrt, L., D. Vickers, J. Sun, T. Crawford, G. Crescenti, and P. Frederickson (2001), Surface stress in offshore flow and quasi-frictional decoupling, *J. Geophys. Res.*, *106*, 20,629–20,639.

Mahrt, L., D. Vickers, P. Frederickson, K. Davidson, and A. Smedman (2003), Sea-surface aerodynamic roughness, *J. Geophys. Res.*, *108*(C6), 3171, doi:10.1029/2002JC001383.

Mahrt, L., D. Vickers, and E. Moore (2004), Flow adjustments across sea-surface temperature changes, *Boundary Layer Meteorol.*, *111*, 553–564.

Mahrt, L., D. Vickers, W. M. Drennan, H. C. Graber, and T. Crawford (2005), Displacement measurement errors from moving platforms, *J. Atmos. Oceanic Technol.*, *22*, 860–868.

Mitsuyasu, H., and T. Kusaba (1996), The effect of swell on certain air-sea interaction phenomena, in *The Air-Sea Interface*, edited by M. A. Donelan, W. H. Hui, and W. J. Plant, pp. 49–53, Rosenstiel School of Mar. and Atmos. Sci., Univ. of Miami, Miami, Fla.

Paulson, C. A. (1970), The mathematical representation of wind speed and temperature profiles in the unstable atmospheric surface layer, *J. Appl. Meteorol.*, *9*, 857–861.

Phillips, O. M., and M. Banner (1974), The effect of swell on the growth of wind waves, *J. Fluid Mech.*, *66*, 625–640.

Pyatt, H. E., A. Albrecht, C. W. Fairall, J. E. Hare, N. Bond, P. Minnis, and J. K. Ayers (2005), Evolution of marine atmospheric boundary layer structure across the cold tongue-ITCZ complex, *J. Clim.*, *18*, 737–753.

Smedman, A. S. (1988), Observations of multi-level turbulence structure in a very stable atmospheric boundary layer, *Boundary Layer Meteorol.*, *44*, 231–253.

Smedman, A. S., M. Tjernstrom, and U. Hogstrom (1994), The near-neutral marine atmospheric boundary layer with no surface shearing stress: A case study, *J. Atmos. Sci.*, *51*, 3399–3411.

Smedman, A. S., H. Bergstrom, and B. Grisogano (1997), Evolution of stable internal boundary layers over a cold sea, *J. Geophys. Res.*, *102*, 1091–1099.

Smith, S. D. (1988), Coefficients for sea surface wind stress, heat flux, and wind profiles as a function of wind speed and temperature, *J. Geophys. Res.*, *93*, 15,467–15,472.

Smith, S. D., et al. (1992), Sea surface wind stress and drag coefficients: The HEXOS results, *Boundary Layer Meteorol.*, *60*, 109–142.

Sun, J., D. Vandemark, L. Mahrt, D. Vickers, T. Crawford, and C. Vogel (2001), Momentum transfer over the coastal zone, *J. Geophys. Res.*, *106*, 12,437–12,448.

Sverdrup, H. U., M. W. Johnson, and R. H. Fleming (1942), *The Oceans*, 1087 pp., Prentice-Hall, Old Tappan, N. J.

Thum, N., S. K. Esbensen, D. B. Chelton, and M. McPhaden (2002), Air-sea heat exchange along the northern sea surface temperature front in the eastern tropical Pacific, *J. Clim.*, *15*, 3361–3378.

Vickers, D., and S. K. Esbensen (1998), Subgrid surface fluxes in fair weather conditions during TOGA COARE: Observational estimates and parameterization, *Mon. Weather Rev.*, *126*, 620–633.

Vickers, D., and L. Mahrt (1997), Quality control and flux sampling problems for tower and aircraft data, *J. Atmos. Oceanic Technol.*, *14*, 512–526.

Vickers, D., and L. Mahrt (1999), Observations of non-dimensional wind shear in the coastal zone, *Q. J. R. Meteorol. Soc.*, *125*, 2685–2702.

Vickers, D., and L. Mahrt (2004), Evaluating formulations of stable boundary layer height, *J. Appl. Meteorol.*, *43*, 1736–1749.

Vickers, D., and L. Mahrt (2006), A solution for flux contamination by mesoscale motions with very weak turbulence, *Boundary Layer Meteorol.*, doi:10.1007/s10546-005-9003-y, in press.

Zilitinkevich, S. S., A. A. Grachev, and C. W. Fairall (2001), Scaling reasoning and field data on the sea surface roughness lengths for scalars, *J. Atmos. Sci.*, *58*, 320–325.

L. Mahrt and D. Vickers, College of Oceanic and Atmospheric Sciences, Oceanography Administration Building 104, Oregon State University, Corvallis, OR 97331-5503, USA. (vickers@coas.oregonstate.edu)